

Flexible Hard Coating: Glass-Like Wear Resistant, Yet Plastic-Like Compliant, Transparent Protective Coating for Foldable Displays

Gwang-Mun Choi, Jungho Jin, Dahye Shin, Yun Hyeok Kim, Ji-Hoon Ko, Hyeon-Gyun Im, Junho Jang, Dongchan Jang,* and Byeong-Soo Bae*

A flexible hard coating for foldable displays is realized by the highly cross-linked siloxane hybrid using structure–property relationships in organic–inorganic hybridization. Glass-like wear resistance, plastic-like flexibility, and highly elastic resilience are demonstrated together with outstanding optical transparency. It provides a framework for the application of siloxane hybrids in protective hard coatings with high scratch resistance and flexibility for foldable displays.

Emerging engineering devices exhibiting unprecedented performance require completely new innovative materials with a nontrivial set of properties that are considered to be inherently incompatible. For example, the development of mechanically deformable display devices such as foldable smartphones that can maintain structural integrity even under high strain conditions requires new optically transparent protective materials that simultaneously attain a high scratch resistance (i.e., hardness) and elastic compliance characteristics, which have been known to be mutually exclusive. Eye-catching prototypes of foldable displays, continually presented by electronics companies or academic organizations in recent years, are convincing people of the prospect that the era of flexible displays is not far from its inauguration.^[1–3] However, the commercialization of high-performance foldable displays is impeded by a crucial technical issue associated with identifying solid substitute for glass cover windows, which have been providing excellent transparency and reliable protection in many optoelectronic engineering devices.^[4] Because of its intrinsic stiffness and brittleness, glass cannot be a leading option for the development and realization of strain-variable optoelectronic devices. A new material-synthesis methodology that imparts high elastic compliance and resilience to silicate glasses without sacrificing their excellent

surface hardness and optical transparency has been required. The combination of a protective hard coating and a transparent plastic film substrate could offer a possible solution to replace traditional brittle silicate glasses for use in flexible cover windows (FCWs). For such a bilayered composite film to be used in FCWs, the transparent coating material should be elastically compliant, should not impede the pliability of

the plastic film and should also be plastically robust in order to ensure excellent resistance against external mechanical impacts and scratches.^[5–7] In other words, the simultaneous attainment of a glass-like wear resistance, a plastic-like modulus, and a high elastic strain limit leading to a remarkable resilience is crucial for coating materials used in FCWs.

The combination of these apparently incompatible mechanical properties, i.e., glass-like wear resistance and plastic-like flexibility, can be achieved by enabling molecular hybridization of materials belonging to different categories such as organics and inorganics,^[8–10] from which our design approach springs. To realize plastic-like modulus, the organic–inorganic (O–I) hybrid materials should have low volume fraction of inorganic phase to organic one. Furthermore, for this hybridization to exhibit glass-like wear resistance and high strength, a crack tip should not be able to distinguish between soft matrix and hard segment in the resultant hybrid, that is, the organic and inorganic phases should be hybridized at the nanometer length scale and the intra-/interphases should also be chemically bonded at the maximum high level. On the basis of the strategy concept, we introduce a newly designed transparent O–I molecular hybrid nanocomposite consisting of siloxane nanobricks covalently linked by epoxy tethers that can act as

G.-M. Choi, Y. H. Kim, J. Jang, Prof. B.-S. Bae
Wearable Platform Materials Technology Center
Department of Materials Science and Engineering
Korea Advanced Institute of Science and Technology (KAIST)
291 Daehak-ro, Yuseong-gu, Daejeon 34141, Republic of Korea
E-mail: bsbae@kaist.ac.kr

G.-M. Choi, J.-H. Ko, Prof. B.-S. Bae
Solip Tech Co., Ltd.
193 Munji-ro, Yuseong-gu, Daejeon 34051, Republic of Korea
Prof. J. Jin
School of Materials Science and Engineering
University of Ulsan
93 Daehak-ro, Nam-gu, Ulsan 44610, Republic of Korea

D. Shin, Prof. D. Jang
Department of Nuclear and Quantum Engineering
Korea Advanced Institute of Science
and Technology (KAIST)
291 Daehak-ro, Yuseong-gu
Daejeon 34141, Republic of Korea
E-mail: dongchan.jang@kaist.ac.kr

Dr. H.-G. Im
Creative and Fundamental Research Division
Korea Electrotechnology Research Institute
12 Bulmosan-ro 10beon-gil
Seongsan-gu, Changwon 51543, Republic of Korea



DOI: 10.1002/adma.201700205

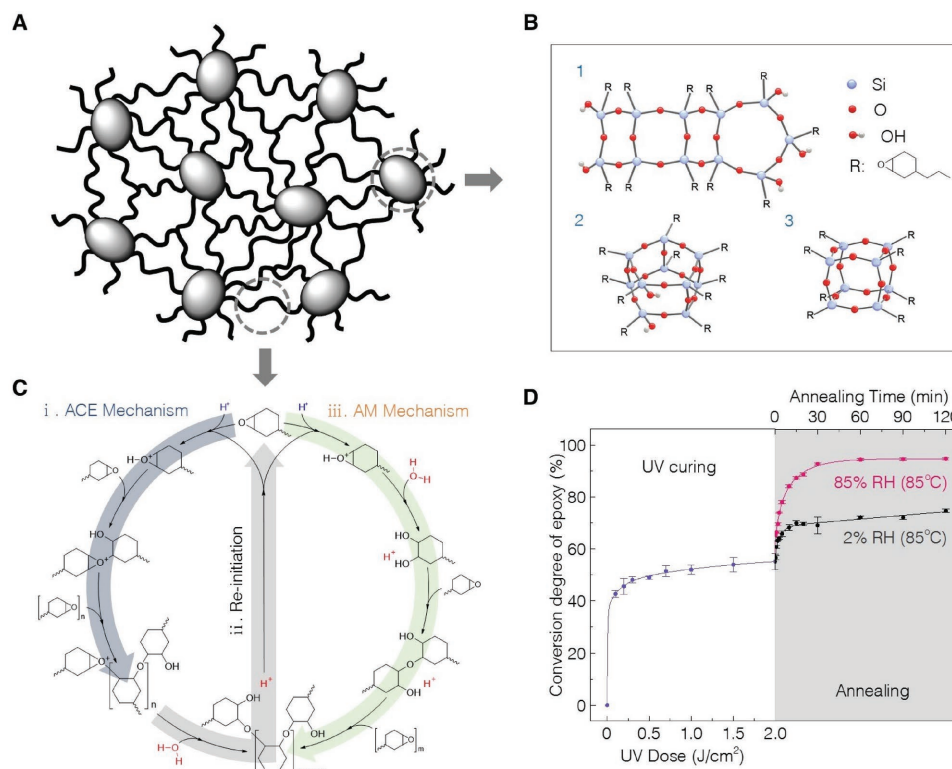


Figure 1. Design concept of the ESMH. A) Schematic illustration of the ESMH consisting of nanosized siloxane molecules densely crosslinked by cycloaliphatic epoxy chains. B) Representative molecular structure of the CEOS (1: ladder-like structure, 2: partial cage, 3: cage). C) CROP of cycloaliphatic epoxides by ACE and AM mechanisms with H₂O molecules as the CTA. D) Epoxy conversion of the CEOS (mean value ± SD, N = 10) upon UV irradiation followed by annealing processes.

a single-phase material as a result of elaborate hybridization, circumventing the trade-off between hardness and flexibility.

Figure 1A shows a schematic illustration of the proposed structure of the epoxy–siloxane molecular hybrid (ESMH) material, which was synthesized by a simple procedure. In the first step, highly condensed siloxane networks with epoxy-organic function were formed using base-catalyzed hydrolysis and the condensation reaction of (2-(3,4-epoxycyclohexyl)ethyl) trimethoxysilane as a synthesis process (Supporting Information). The synthesis produced a clear, viscous semiliquid material exhibiting a high degree of condensation (≈97%), as determined by liquid-state ²⁹Si NMR analysis (Figure S1A, Supporting Information). To further examine the structure at the molecular level, spectroscopic studies using Fourier transform infrared (FTIR) spectroscopy, dispersive-Raman spectroscopy, and matrix-assisted laser desorption/ionization time-of-flight mass spectrometry (MALDI-TOF-MS) were performed (Figure S1B–D and Table S1, Supporting Information). These studies revealed that the product consists of cycloaliphatic epoxy-functionalized oligosiloxanes (CEOS), among which the dominant species is a ladder-like silsesquioxane consisting of 11 Si atoms; other species of different structures such as cage and partial-cage structures are also included (Figure 1B and Supporting Information).

Next, the CEOS nanobuilding blocks were converted into a monolithic material consisting of organic (epoxy) and inorganic (siloxane) networks chemically bonded to each other, obtained

from UV-initiated cationic ring-opening polymerization (CROP) of the CEOS's epoxides.^[11] However, despite its living characteristics, in the CROP of multifunctional molecules (e.g., CEOS), a fully crosslinked network is not straightforward owing to the isolation of growing chains in the polymeric matrix.^[12,13] The ESMH with highly crosslinked epoxy networks was realized by the following process: addition of an onium salt as a photoinitiator to the CEOS, UV irradiation (≈2 J cm⁻²) onto the mixture at ambient atmosphere, and moisture annealing of the UV-cured material in a humid box (85 °C, 85% RH) for 2 h (Supporting Information). The corresponding degree of epoxy conversion was simultaneously calculated from the FTIR spectra (Figure 1D and Supporting Information). The post moisture annealing drastically increased the epoxy conversion of the CEOS from ≈55% at the end point of UV curing up to ≈95%, whereas virtually moisture-free conditions (85 °C, 2% RH) resulted in limited epoxy conversion (≈75%). This boost of the crosslinking reaction was designed using two competitive mechanisms of CROP,^[14–16] active-chain end (ACE), and active monomer (AM), which were sequentially combined using H₂O as a chain-transfer agent (CTA) (Figure 1C). In the near absence of CTA during UV curing, polymeric chains are formed by the ACE mechanism, and the chain propagation rate gradually decreases owing to the trapped active center of tertiary oxonium ions in the network (i). The diffusion of H₂O into the reaction-limited matrix by moisture annealing leads to a reaction between the tertiary oxonium ion and the water

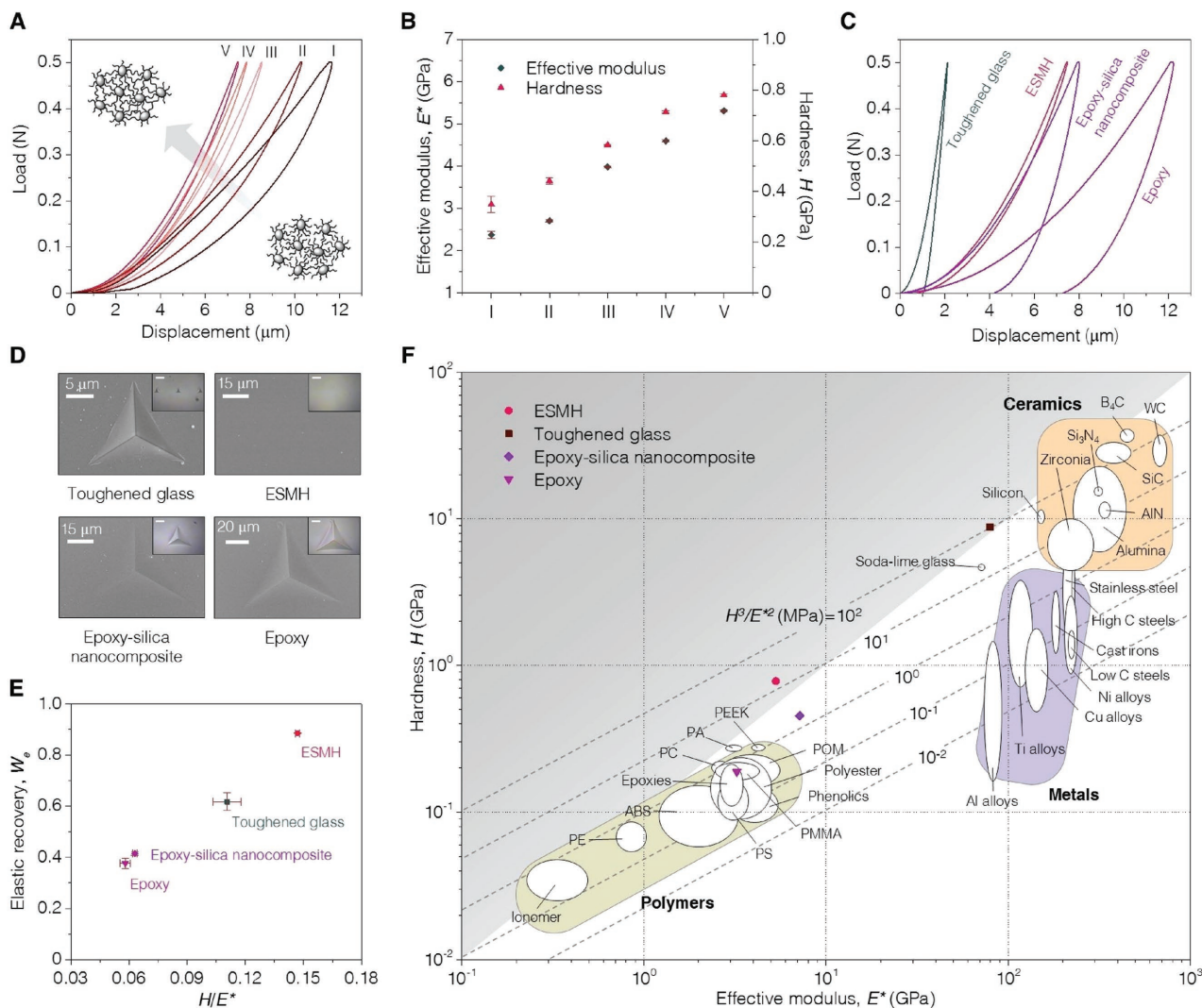


Figure 2. Nanoindentation characterization of the ESMH. A) Representative load–displacement curves according to changes in the crosslinking between the CEOS nanobuilding blocks. B) The increase of cross-linking density leads to an enhancement of the effective modulus and hardness concurrently, shown as mean \pm SD ($N = 9$). C) Representative load–displacement curves for indentations in the ESMH, the toughened glass, the epoxy–silica nanocomposite, and the epoxy. D) SEM and OM images of residual impressions after the indentation tests (C). The scale bar in the insets is 20 μm . E) A plot of the elastic recovery versus hardness-to-effective modulus ratio. (Data are presented as mean \pm SD, $N = 9$.) F) Ashby map of hardness versus effective modulus for estimation of wear resistance, showing that the ESMH reaches a new domain marked by the high-hardness and -compliance. Reproduced with permission.^[40] Copyright 2007, Elsevier Ltd. The upper left shaded area is the region satisfying $H/E^* \geq 0.1$.

molecule, yielding a hydroxyl end group and an acidic proton that reinitiates a neutral epoxide (ii), producing a new secondary oxonium ion. With the abundance of H_2O as the CTA, epoxy polymer chains grow again by the AM mechanism (iii). This well-controlled curing process is capable of generating the maximally polymerized organic phase in the ESMH. Furthermore, during moisture annealing (ii and iii), the injected H_2O molecules expand the volume of the system, which can compensate for volume shrinkage inevitably induced by the ACE polymerization during UV curing (i). This result was clearly confirmed by FTIR analysis and by curvature changes in the coating film during the curing process (Figures S2 and S3, Supporting Information).

The fabricated ESMH with thickness of 50 μm , of which an Archimedean density is $\approx 1.30 \text{ g cm}^{-3}$ resulting from the low

inorganic volume fraction, shows the excellent optical properties over the visible region: $\approx 91.4\%$ parallel transmittance and $\approx 8.1\%$ total reflectance at 450 nm characterized by UV–Vis spectra (Figure S4A, Supporting Information); haze values of less than 0.15 measured by a haze meter (Table S2, Supporting Information). The outstanding transparency is attributed to a nanometer-scale-hybridization,^[17] as evidenced from the high-resolution transmittance electron microscopy image and the corresponding energy dispersive X-ray spectroscopy 2D mapping results of Si, O, and C, which reveals that the material is in a wholly amorphous state having a similar, homogeneous distribution of Si, O, and C (Figure S4B, Supporting Information). In nanometer scale, organic and inorganic phases are indistinguishable, which makes the ESMH sufficiently transparent to be applicable to optical coatings.

To evaluate the mechanical potential of the ESMH for wear resistant coatings, we performed nanoindentation experiments based on the Oliver–Pharr method.^[18] Figure 2A shows nanoindentation load (P)–displacement (h) curves of specimens with different crosslinks between the CEOS nanobuilding blocks, i.e., conversion degrees of epoxy: I ($30.3 \pm 2.6\%$), II ($49.4 \pm 0.6\%$), III ($65.5 \pm 1.3\%$), IV ($75.3 \pm 0.6\%$), and V ($94.6 \pm 0.4\%$) corresponding to that of the ESMH (Supporting Information). The higher the conversion degree of epoxy, the smaller is a hysteresis of the P – h curve, revealing higher elastic resilience. Furthermore, with increasing the crosslinking ($I \rightarrow V$), the nanoindentation hardness (H) increased from 0.35 ± 0.03 to 0.78 ± 0.01 GPa and the effective modulus (E^*) increased from 2.37 ± 0.08 to 5.31 ± 0.02 GPa, as shown in Figure 2B and Table S3 (Supporting Information), where $E^* = E/(1 - \nu^2)$; E is the Young's modulus and ν is the Poisson's ratio.

For a comparative study, we also tested following reference specimens: a toughened glass as the inorganic part; an epoxy–silica nanocomposite without any covalent bond between organic and inorganic phases as the counterpart of the ESMH; and an epoxy as the organic part (Supporting Information). Figure 2C indicates nanoindentation P – h curves of the test specimens, showing that the ESMH exhibited the smallest hysteresis of the curve. Besides, the nanoindentation could not induce clear permanent deformation on the ESMH contrary to other reference ones, as confirmed by optical microscopy (OM) and scanning electron microscopy (SEM) images (Figure 2D). Quantitatively, the mechanical properties such as E^* , H , and the elastic recovery (W_e) were calculated

and summarized in Table S3 (Supporting Information). The significance of H/E^* and W_e are stressed as key parameters that are necessary for the flexible hard nanocomposite coatings.^[7] The materials with a low value of E^* satisfying $H/E^* \geq 0.1$ and $W_e \geq 60\%$ generate hard, tough and resilient coatings with enhanced resistance to cracking. Figure 2E shows a plot of W_e against H/E^* of the test specimens. It is noteworthy that the ESMH simultaneously attains plastic-like low E^* with exceptionally high $H/E^* = 0.147 \pm 0.001$ and $W_e = 88.5 \pm 0.1\%$. To illustrate the uncommon properties of the ESMH, a material selection chart of H against E^* for engineering materials is shown in Figure 2F. The diagonal dashed lines indicate the selection criteria according to the value of H^3/E^{*2} , which is directly related to resistance against yield pressure, i.e., wear resistance.^[19,20] Due to the combination of high H and low E^* , the H^3/E^{*2} value of the ESMH exceeds the highest value of polymers and compares to those of ceramics such as a soda-lime glass, which means the ESMH is highly suitable for the wear resistant coatings. Note that for highly resilient materials such as the ESMH, it is known that accuracy of the values of E^* , H obtained from nanoindentation experiments may be compromised. However, because all the data in Figure 2F was determined by the same experimental approach, the qualitative comparison is considered to be valid.

To investigate the mechanical responses of the ESMH under varying strain conditions it will encounter during the actual applications as flexible protective coatings, we conducted in situ bending experiments by applying monotonic (Figure 3, top) or cyclic (Figure 3, bottom) loading at the center of doubly

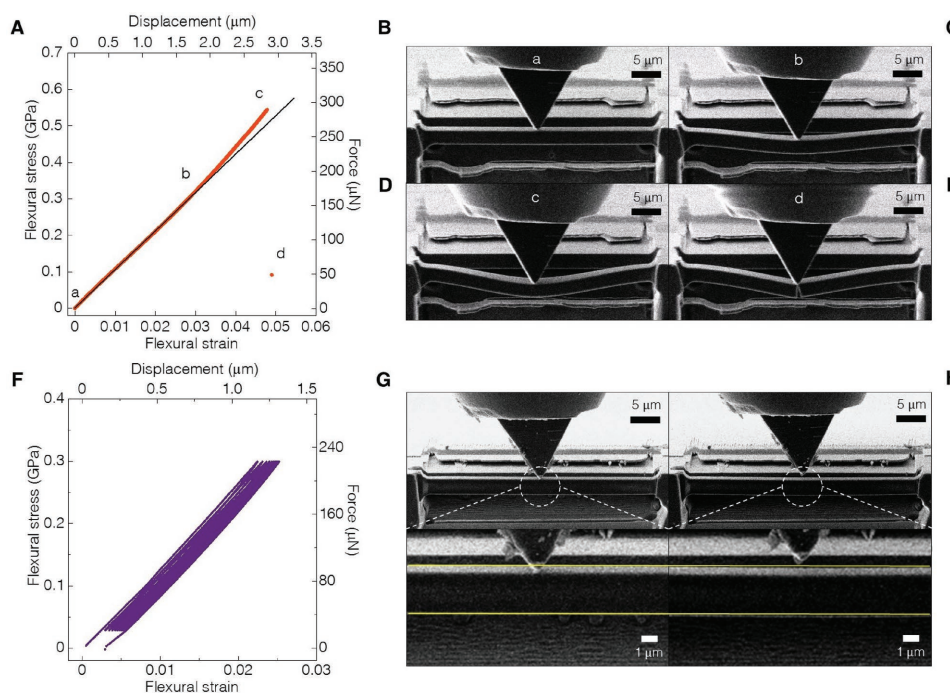


Figure 3. Three-point bending results for doubly clamped microbeam-shaped ESMH. A) Representative flexural stress–strain (force–displacement) curve from the monotonic bending tests. B–E) In situ SEM images recorded during the corresponding test at σ values of 0 GPa (B), 0.35 GPa (C), and 0.55 GPa (D), and at fracture (E). F) Flexural stress–strain (force–displacement) curve from the cyclic bending test. G, H) SEM images before (G) and after (H) the cyclic bending test. The straight yellow lines were used to determine the extent of deformation. We assume that the minuscule residual bending is related to viscoelastic and/or plastic deformation arising from the high local stresses at both ends of the beam.^[41]

clamped microbeams fabricated by focused-ion-beam (FIB) milling. Figure 3A shows representative flexural stress–strain (force–displacement) data obtained in monotonic tests (Supporting Information). SEM images captured in the course of monotonic bending tests are presented in Figure 3B–E, for the initial contact (a), onset of nonlinearity (b), maximum stress (c), and after fracture (d) (for the full in situ video, see Movie S1 in the Supporting Information). The curve shows nearly linear elastic behavior over the entire loading cycle prior to fracture, with the exception of a slight deviation from the initial linearity in regime b–c, which is likely due to the geometric constraint effect at fixed ends in the beam structure (Section 2 in Supporting Information). Although the general characteristics of the curve, such as the initial linear loading followed by a failure, may appear to be phenomenologically similar to those of typical ceramics, it should be noted that the total elastic strain at fracture in Figure 3A significantly exceeds the values obtained for typical ceramics^[21] ($\approx 0.1\%$) owing to the large amount of energy absorbed purely by elastic deformation. Based on quantitative measurements, the obtained Young's modulus (E) and strength (σ_f) of our ESMH are 10.8 ± 0.5 GPa and 544.09 ± 104.08 MPa, respectively, leading to a modulus of resilience $U_r = 13.06 \pm 3.74$ MJ m^{-3} (Table S4, Supporting Information). The reliability of Young's modulus measured by the bending experiment, which is discernibly different from the nanoindentation

value, was confirmed using a finite-element method framework under the same experimental condition (Figure S5, Supporting Information). To the best of our knowledge, no engineering material attaining such a unique combination of high strength and low modulus has previously been reported.^[22] To further investigate the elastic recoverability of the ESMH, a cyclic bending experiment was performed by sequentially repeating 15 loading–unloading cycles on a sample with a geometry identical to that used in the monotonic testing (Figure 3F–H and Movie S2, Supporting Information). In each cycle, the microbeam specimen was loaded up to $\approx 60\%$ of the predetermined average fracture load obtained from the previous monotonic loading tests and was subsequently unloaded down to 10% of the maximum load. Figure 3F shows the resultant flexural stress–strain and force–displacement curves, demonstrating the considerable elastic recoverability of the material with only a slight residual deflection of up to ≈ 150 nm after 15 cycles. The SEM images (Figure 3G,H) visually support this observation as well. The experimental observations under the monotonic and cyclic loading conditions imply that the material is quite strong but can be easily deformed and restored to its original shape, making ESMH an ideal candidate for use in strain variable coatings.

An Ashby's material property chart plotting E against σ_f is shown in Figure 4 to compare the mechanical properties

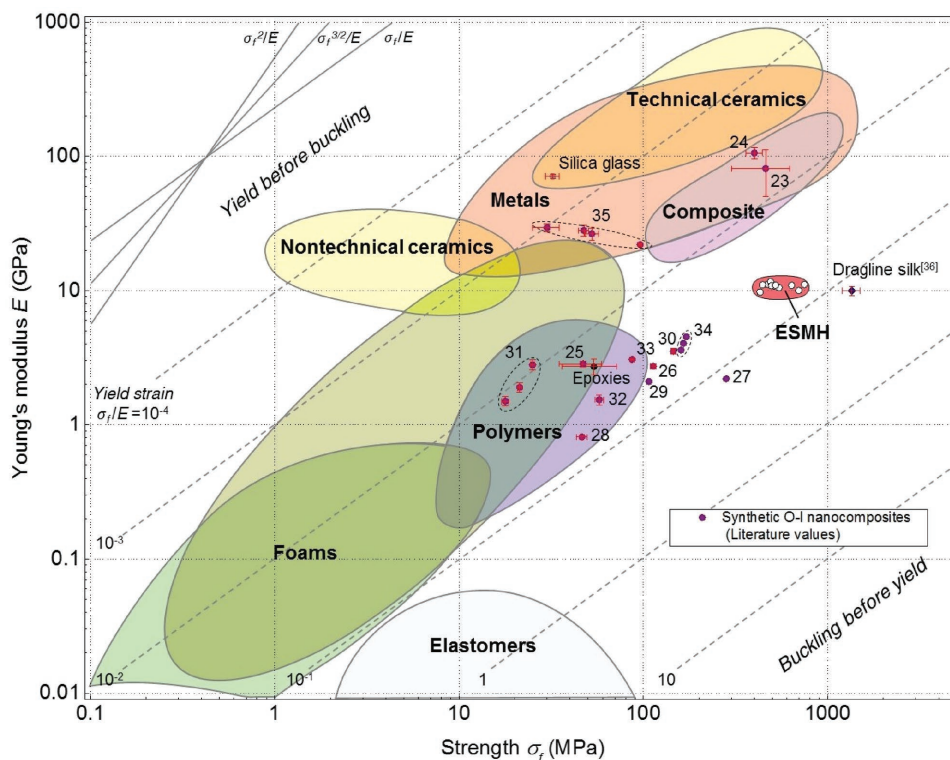


Figure 4. Material property map plotting Young's modulus against strength. (Reproduced with permission.^[22] Copyright 2011, Elsevier Ltd.) The diagonal parallel dashed lines correspond to contours of fracture strain, σ_f/E . Owing to its high strength and low modulus, the ESMH undoubtedly belongs to a regime comparable to that of dragline silk,^[36] which has not been previously reached by any other common engineering material. Literature values for other synthetic O–I nanocomposites are given. O–I nanocomposites with covalent linkages between organic and inorganic components: iron oxide/oleic acid nanocomposite,^[23] poly(vinyl alcohol)/montmorillonite clay nanocomposite,^[24] chitosan/silica nanocomposite,^[25] polyimide/silicate nanocomposite,^[26] (hydroxyethyl)methacrylate/silica nanocomposite,^[27] and polyurethane/silica nanocomposite.^[28] O–I nanocomposites without covalent bonds between organic and inorganic components: nylon/silicate nanocomposite,^[29] epoxy/alumina nanocomposite,^[30] and epoxy/silica nanocomposites.^[31–35]

obtained in the bending experiments with the known data for all existing engineering materials and other synthetic O–I nanocomposites.^[23–35] It is clear that our results create a new domain characterized by high σ_f and low E with a polymer-level failure strain, $\sigma_f/E \sim 0.05$; only a few natural materials such as dragline silk exhibit comparable values.^[36] These unusual properties can be understood in terms of the composite modulus (E') and strength (σ_f') of the multiphase material. For simplicity, the ESMH is regarded as a two-phase nanocomposite comprising a cycloaliphatic epoxy matrix with dispersed silica nanoparticles, for which E' can be estimated from the Hashin–Shtrikman (H–S) bounds.^[37] The theoretically expected E' ranges from 4.5 to 10.1 GPa (Figure S7, Supporting Information), indicating that the experimentally determined E of the ESMH corresponds to the H–S upper bound, the highest value for a given system. In contrast, in the case of σ_f' , an increase in the volume fraction of the reinforcing agents results in poor enhancement.^[38,39] However, as shown in Figure 4, our system exhibits increases of a factor of three and a factor of ten in E and σ_f , respectively, compared with commercial epoxy polymers. We interpret this phenomenon as a combined effect of the molecular level hybridization and covalent bonding between phases, which causes the composite to behave as an effectively strengthened single-phase material at the scale of the crack-tip stress field. Consequently, the enhanced E is the primary factor leading to the increase in σ_f according to linear elastic fracture mechanics while maintaining a polymer-like σ_f/E ratio.

To evaluate the potential use of ESMH in foldable hard coatings, a 50 μm thick ESMH coating was fabricated on a commercial 75 μm thick polyethylene terephthalate (PET) film (Figure 5A). The coated film shows a high surface pencil hardness of 9H, which is comparable to that of the glass surface (Figure S8, Supporting Information). Furthermore, as shown in Figure 5B–E, the film achieved remarkable performance for application as an FCW for foldable devices: excellent flexibility for concave folding to a radius of curvature of 1 mm over more than 10 000 cycles without permanent deformation or fracture (Figure 5B,C and Movie S3, Supporting Information); extreme elastic recoverability in nearly restoring its original shape, as confirmed by nanoscratch (Figure 5D), nanoindentation (Figure 2C,D), microbeam cyclic bending (Figure 3F–H), and micro-Vickers hardness tests (Figure S9, Supporting Information); and outstanding wear resistance, as revealed by an industrial steel-wool abrasion test result (Figure 5E and Movie S4), whereas the epoxy–silica nanocomposite coating showed poor wear resistance (Figure S10, Supporting Information).

In summary, we have demonstrated an authentic O–I hybrid that simultaneously realizes all of the benefits of both flexible and wear resistant materials; moreover, this hybrid can be fabricated by a simple, mass-producible and low-energy-consuming method based on the strategy of hybridization to increase the chemical bonds of intra- and interphases at the molecular level. Because of the unique combination of intrinsic properties such

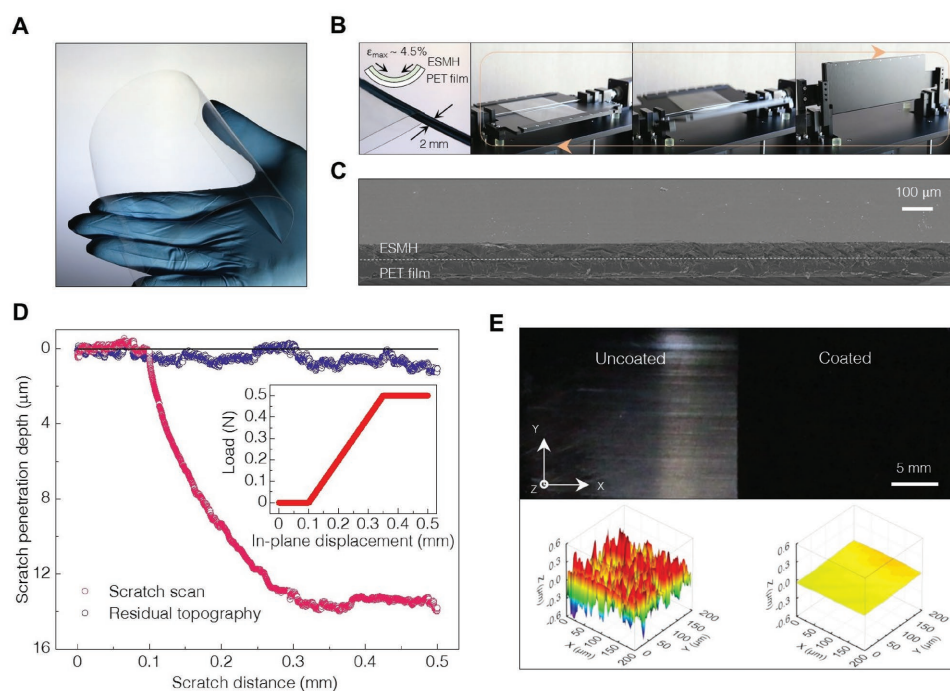


Figure 5. Application of the ESMH as a foldable hard coating on a plastic substrate. A) Photograph of the ESMH coated on a PET film. B) Dynamic folding test of the ESMH coated on a PET film. C) Panoramic SEM image after the folding test, showing the region repeatedly folded and unfolded. D) Scratch penetration depth–scratch distance curves from the nanoscratch test with a Berkovich tip. The scratch scan data show the on-load penetration depth, which is the sum of elastic and plastic deformation. After the removal of the scratch load, the penetrated depth was nearly recovered, and a small amount of plastic deformation was retained, as shown in the residual topography data. The inset shows a corresponding load profile during the scratch scan. E) Steel-wool wear test of the ESMH coated on a PET film. The photograph (top) clearly shows that visual scratches are only observed on the uncoated side. White-light scanning interferometric images (bottom) clearly demonstrate that the ESMH is absolutely free of scratches (the coordinate system corresponds to the one shown in the photograph).

as high wear resistance and strength, low modulus and optical transparency, our findings create a new option for material selection that can surmount technical barriers for the commercialization of flexible and even foldable optoelectronics.

Supporting Information

Supporting Information is available from the Wiley Online Library or from the author.

Acknowledgements

This research was supported by Wearable Platform Materials Technology Center (WMC) funded by the National Research Foundation of Korea (NRF) Grant of the Korean government (MSIP) (No. 2016R1A5A1009926). This work was also supported by the National Research Foundation of Korea (NRF) Grant funded by the Korean government (MSIP) (NRF-2014R1A2A2A01005009) and the INNOPOLIS Foundation funded by the Korea government (MSIP) (A2014DD102).

Received: January 10, 2017

Revised: February 12, 2017

Published online:

- [1] H. Shim, I. Kee, S. Kim, Y. Chun, H. Kwon, Y. Jin, S. Lee, D. Han, J. Kwack, D. Kang, H. Seo, M. Song, M. Lee, S. Kim, *SID Symp. Dig. Tech. Pap.* **2010**, 41, 257.
- [2] J. Chen, J. Ho, G. Chen, M. Yeh, Y.-Z. Lee, C. Lee, *SID Symp. Dig. Tech. Pap.* **2016**, 47, 1041.
- [3] X. Huang, K. Hu, L. Lin, Q. Shan, X. Yang, X. Gao, *SID Symp. Dig. Tech. Pap.* **2016**, 47, 412.
- [4] J. C. Mauro, C. S. Philip, D. J. Vaughn, M. S. Pambianchi, *Int. J. Appl. Glass Sci.* **2014**, 5, 2.
- [5] A. Leyland, A. Matthews, *Wear* **2010**, 246, 1.
- [6] N. Holten-Andersen, G. E. Fantner, S. Hohlbauch, J. H. Waite, F. W. Zok, *Nat. Mater.* **2007**, 6, 669.
- [7] J. Musil, *RSC Adv.* **2015**, 5, 60482.
- [8] H. Gao, B. Ji, I. L. Jager, E. Arzt, P. Fratzl, *Proc. Natl. Acad. Sci. USA* **2003**, 100, 5597.
- [9] R. O. Ritchie, *Nat. Mater.* **2011**, 10, 817.
- [10] C. Sanchez, H. Arribart, M. M. Giraud Guille, *Nat. Mater.* **2005**, 4, 277.
- [11] S. Aoshima, S. Kanaoka, *Chem. Rev.* **2009**, 109, 5245.
- [12] S. Penczek, M. Cypryk, A. Duda, P. Kubisa, S. Slomkowski, *Prog. Polym. Sci.* **2007**, 32, 247.
- [13] J. V. Crivello, R. Malik, *J. Polym. Sci., Part A: Polym. Chem.* **1997**, 35, 407.
- [14] R. Tokar, P. Kubisa, S. Penczek, A. Dworak, *Macromolecules* **1994**, 27, 320.
- [15] C. Decker, T. Nguyen Thi Viet, H. Pham Thi, *Polym. Int.* **2001**, 50, 986.
- [16] P. Kubisa, S. Penczek, *Prog. Polym. Sci.* **1999**, 24, 1409.
- [17] J. Wen, G. L. Wilkes, *Chem. Mater.* **1996**, 8, 1667.
- [18] W. C. Oliver, G. M. Pharr, *J. Mater. Res.* **1992**, 7, 1564.
- [19] T. Y. Tsui, G. M. Pharr, W. C. Oliver, C. S. Bhatia, R. L. White, S. Anders, A. Anders, I. G. Brown, *MRS Proc.* **1995**, 383, 447.
- [20] K. L. Johnson, *Contact Mechanics*, Cambridge University Press, Cambridge, UK **1985**, p. 155.
- [21] W. D. Callister, *Fundamentals of Materials Science and Engineering: An Integrated Approach*, John Wiley & Sons, Hoboken, NJ, USA **2005**.
- [22] M. F. Ashby, *Materials Selection in Mechanical Design*, Butterworth-Heinemann, Oxford, UK **2011**.
- [23] A. Dreyer, A. Feld, A. Kornowski, E. D. Yilmaz, H. Noei, A. Meyer, T. Krekeler, C. Jiao, A. Stierle, V. Abetz, H. Weller, G. A. Schneider, *Nat. Mater.* **2016**, 15, 522.
- [24] P. Podsiadlo, A. K. Kaushik, E. M. Arruda, A. M. Waas, B. S. Shim, J. Xu, H. Nandivada, B. G. Pumpllin, J. Lahann, A. Ramamoorthy, N. A. Kotov, *Science* **2007**, 318, 80.
- [25] Y.-L. Liu, Y.-H. Su, J.-Y. Lai, *Polymer* **2004**, 45, 6831.
- [26] C.-M. Leu, Z.-W. Wu, K.-H. Wei, *Chem. Mater.* **2002**, 14, 3016.
- [27] B. M. Novak, *Adv. Mater.* **1993**, 5, 422.
- [28] C. Y. Bae, J. H. Park, E. Y. Kim, Y. S. Kang, B. K. Kim, *J. Mater. Chem.* **2011**, 21, 11288.
- [29] E. P. Giannelis, *Adv. Mater.* **1996**, 8, 29.
- [30] B. Wetzels, P. Rosso, F. Hauptert, K. Friedrich, *Eng. Fract. Mech.* **2006**, 73, 2375.
- [31] M. Pregonella, A. Pegoretti, C. Migliaresi, *Polymer* **2005**, 46, 12065.
- [32] L. Chen, S. Chai, K. Liu, N. Ning, J. Gao, Q. Liu, F. Chen, Q. Fu, *ACS Appl. Mater. Interfaces* **2012**, 4, 4398.
- [33] C. M. Manjunatha, A. C. Taylor, A. J. Kinloch, S. Sprenger, *Compos. Sci. Technol.* **2010**, 70, 193.
- [34] T. Mahrholz, J. Stängle, M. Sinapius, *Composites, Part A* **2009**, 40, 235.
- [35] P. L. Teh, M. Mariatti, H. M. Akil, C. K. Yeoh, K. N. Seetharamu, A. N. R. Wagiman, K. S. Beh, *Mater. Lett.* **2007**, 61, 2156.
- [36] U. G. K. Wegst, M. F. Ashby, *Philos. Mag.* **2004**, 84, 2167.
- [37] Z. Hashin, S. Shtrikman, *J. Mech. Phys. Solids* **1963**, 11, 127.
- [38] M. A. Osman, J. E. P. Rupp, U. W. Suter, *Polymer* **2005**, 46, 1653.
- [39] S. Mishra, A. K. Mohanty, L. T. Drzal, M. Misra, S. Parija, S. K. Nayak, S. S. Tripathy, *Compos. Sci. Technol.* **2003**, 63, 1377.
- [40] F. W. Zok, A. Miserez, *Acta Mater.* **2007**, 55, 6365.
- [41] W. D. Pilkey, D. F. Pilkey, *Peterson's Stress Concentration Factors*, John Wiley & Sons, Hoboken, NJ, USA **2007**.